Structural origin of the x-ray diffuse scattering in $(CH_3)_4NCdCl_3$ and related compounds

Marek Paściak, Marek Wołcyrz, and Adam Pietraszko
Institute of Low Temperature and Structure Research, Polish Academy of Sciences, P.O. Box 1410, Wrocław 2, Poland
(Received 14 March 2008; revised manuscript received 27 May 2008; published 22 July 2008)

The local structure of $(CH_3)_4NCdCl_3$ (TMCC) has been determined by a configurational-bias reverse Monte Carlo method applied to x-ray diffuse scattering data. The following two phases have been analyzed and refined: phase I at 293 K, $P6_3/m$ space group, $a=9.139(1)$Å, and $c=6.723(1)$Å; and phase I′ at 410 K, $P6_3/mmc$ space group, $a=9.235(1)$Å, and $c=6.742(1)$Å. A model dividing the $CdCl_6$ octahedral chains into elementary blocks has been implemented in order to take into account the coupling between the orientation of the $(CH_3)_4N$ molecules and the local deformations of the octahedral chains. The resulting structures contain subchains of $CdCl_6$ octahedra that are shifted longitudinally away from their average positions. The subchain lengths can be described by a Poisson-like distribution with an average length of roughly six unit cells. X-ray diffuse scattering effects observed on the *hk*0 plane require the existence of transverse subchain displacements. An additional correlation between the transverse and longitudinal shifts of the subchains was needed in order to explain the weak modulation effects and diffuse streaks observed on the planes perpendicular to c^*.

DOI: 10.1103/PhysRevB.78.024114 PACS number(s): 61.43.Bn, 61.05.C−, 61.66.−f

I. INTRODUCTION

$(CH_3)_4NCdCl_3$ (TMCC) together with $(CH_3)_4NMnCl_3$ (TMMC), $(CH_3)_4NNiCl_3$ (TMNC), and $(CH_3)_4NMnBr_3$ (TMMB) belong to a large group of compounds of the type $(CH_3)_4NMX_3$, where M is a bivalent metal (M =Mn, Ni Cd, Cu, V, Pb) and X is a halogenide (X=Cl, Br, or I). Representatives of this group where M is a magnetic element were widely studied in 1970s and 1980s because of their quasi-ideal one-dimensional magnetic properties.[1–5]

The crystal structure of TMCC and related compounds (Fig. 1) is composed of isolated infinite linear chains of face-shared MX_6 octahedra, which are widely separated by tetramethylammonium (TMA) molecules, $(CH_3)_4N$ (Refs. 6–10). A complex network of hydrogen bonds is spanned between the TMA molecules and the octahedral chains. All of the compounds in this group undergo several structural phase transitions as a function of temperature.[1,7–17]

In the case of TMCC, two successive structural phase transitions have been observed at 118 and 104 K. Phase I (using the phase numbering scheme of Braud *et al.*[8]) is hexagonal ($P6_3/m$ space group and $Z=2$) at room temperature. Below 118 K, this structure transforms into a ferroelastic monoclinic phase III ($P2_1/m$ space group and $Z=2$). At 104 K it transforms to another monoclinic phase IV ($P2_1/b$ space group and $Z=12$). Instead of phases III and IV, only one—phase II ($P2_1/b$ space group, $Z=4$)—exists below 126 K for TMMC. In TMCC at 400 K, phase I transforms into the higher-symmetry hexagonal phase I′ ($P6_3/mmc$ space group,

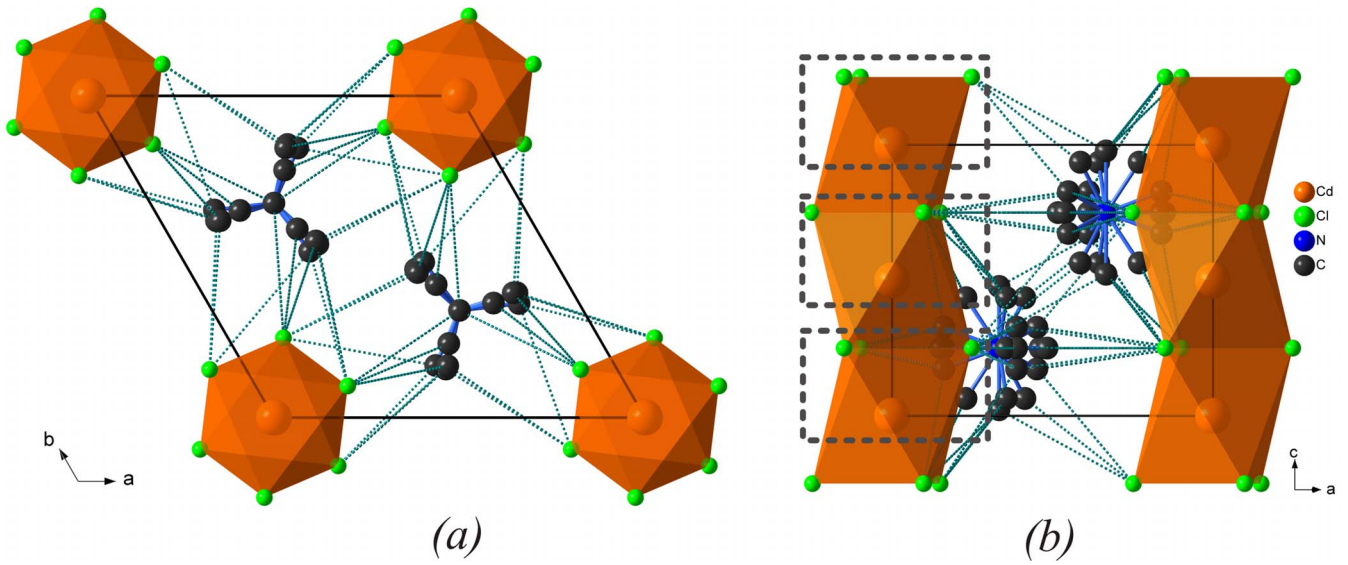

FIG. 1. (Color online) The crystal structure of the room-temperature phase I of TMCC and related compounds: (a) the projection on *ab* plane and (b) a view along *b* direction. Chains of the $CdCl_6$ octahedra and the disordered TMA molecules are shown. A net of possible hydrogen bonds binding the TMA molecules and the $CdCl_6$ octahedral chains is shown. The hydrogen atoms are omitted. A division of the chain into elementary blocks used in the refinement (see Sec. V) is shown in (b).

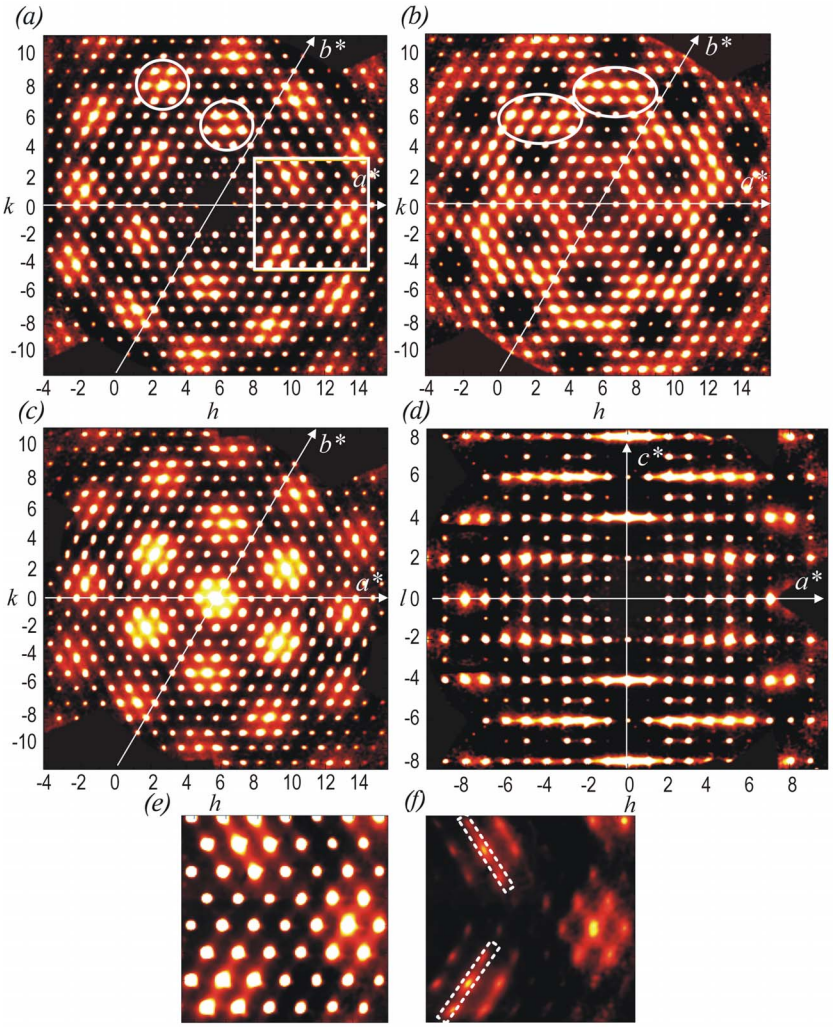

FIG. 2. (Color online) Experimental sections of the reciprocal space observed in TMCC at room temperature, which contains Bragg reflections and XDS. Four sections are shown: (a) $hk0$, (b) $hk2$, (c) $hk4$, and (d) $h0l$. The selected areas of the strong modulation in the XDS intensity are indicated by circles and ellipses in (a) and (b). The weak modulations effects, seen in the square in (a), are magnified in (e) as they are in $hk0$. (f) $hk0.3$ section with the XDS streaks indicated by dotted line rectangles.

$Z=2$, and $BaNiO_3$ structure type), which is the aristotype for all compounds considered in this work.

It was shown that the observed phase sequence is characterized by an antiphase translational displacement of the infinite linear chains along the hexagonal axis, which couples with an orientational ordering process of the TMA molecules. The latter process can be described in the framework of a complex Frenkel model involving the reorientation of the TMA molecules over two, three, five, or six energetically equivalent potential wells in the room-temperature phase. In phase I′, there are twice as much orientations accessible to the TMA molecules.

There are relatively few papers on solving and refining the crystal structure of TMCC and related compounds. The main obstacles for solving these crystal structures arise from the complex nature of structural disorder at high temperatures and from the fact that the ferroelasticity of the crystals leads to a twinning at low temperatures. The room-temperature phase has been refined by several authors on single crystals and on powders[6–10] but there is no common agreement for the model of TMA disorder. There have only been a few refinement trials of the low-temperature phases but the results were either incomplete[8,10] or were obtained on a powder sample only.[9]

It should be mentioned that all of the above cited structural papers (with the exception of Ref. 8) used a routine crystal structure analysis for obtaining an average crystal structure. Therefore, they did not take into account a great part of the structural information provided by the x-ray diffuse scattering (XDS), which directly relates to the structural disorder appearing in the crystal. The only description and interpretation of these phenomena was given in a paper by Braud *et al.*[8] where they pointed out that the strong effects observed in XDS experiments were mostly caused by static $CdCl_6$-chain disorder instead of the disordered network of light TMA molecules. They proposed a model consisting of translational displacements of the octahedral chains along the c axis, which explained the three most important XDS effects that were experimentally observed: (i) the width of the observed diffuse planes that extend perpendicularly to the c^* direction is associated with intrachain correlations {around 18—23 unit cells along the c axis [see Fig. 2(d)]}, (ii) the "strong modulations" of intensity in the diffuse planes were assigned to the shape factor of the chain [see Figs. 2(a) and 2(c)], and (iii) additional "weak modulations" of intensity were attributed to the existence of interchain correlations {6—9 unit cells in ab plane [see Fig. 2(e)]}.

Although valuable from a scientific point of view, the paper by Braud *et al.*[8] contained many simplifying assumptions

and left many unanswered questions. First of all, they did not interpret the experimentally observed XDS effects existing in the $hk0$ reciprocal plane, which could not be explained by using their model. Second, they did not provide an explanation for the additional weak modulation seen in the reciprocal planes perpendicular to c^*. Finally, their methodology was limited only to simple modeling. They obtained only qualitative and not quantitative agreement with the experimental data.

In the present paper, we develop and improve the approach applied by Braud *et al.*[8] by extending their model of the chain disorder to include transverse chain displacements and their local distortions. Moreover, we perform a stricter quantitative refinement of the local structure using the reverse Monte Carlo procedure (RMC) based on the XDS data. Both of these improvements lead to a more realistic picture and insight for the nanoscale structure of disordered TMCC and related compounds. We also consider another possible explanation of the XDS effects based on the theory of thermal diffuse scattering given by Komatsu and Teramoto.[18] According to their interpretation, nonradial XDS can originate (in certain classes of compounds) from low-frequency transverse lattice waves with wave-number vectors that are perpendicular to the atomic chains present in crystal. We combine arguments from both interpretations (static and dynamic) and present our local structure determination in the light of both models.

II. EXPERIMENT

Single crystals of TMCC were grown from an acidic aqueous solution of $(CH_3)_4NCl$ and $CdCl_2$ by slow evaporation at room temperature. Good quality crystals with a size of $0.21\times0.25\times0.29$ mm^3 were chosen for the x-ray diffraction experiments. Data collections for both conventional crystal structure analysis and XDS refinement were performed on an Oxford Diffraction Xcalibur four-circle single-crystal diffractometer, which was equipped with a CCD camera and a graphite-monochromatized MoK_α radiation ($\lambda=0.71073$ Å) generated at 50 kV. A 25 mA current was used in the experiments. For high-temperature measurements at 410 ± 0.5 K, an Oxford Diffraction high-temperature blowing system of hot air was applied. Moreover an Oxford Cryosystem liquid nitrogen attachment was applied for the measurements in the low-temperature range (100—300 K), which provided a temperature stability of ±1 K.

Three-dimensional sets of x-ray diffraction data were collected in 1611 frames in the 2θ range of $3°-92°$ with $\Delta\omega=1.2°$, and the recording time for a single frame was 40 s. The lattice parameters were calculated from the positions of all measured reflections. The intensities of the Bragg reflections for an average structure refinement were corrected for both the Lorentz and polarization factors. Moreover an analytical absorption correction was also applied. The total number of collected reflections was 8268 for the measurements at 293 K and 6749 for the measurements at 410 K.

A conventional x-ray crystal structure analysis was performed by means of the SHELX-97 software package.[19] Twenty reciprocal planes were extracted for the analysis of the XDS from the set of registered frames with the help of CRYSALIS software.[20] The background was subtracted by routine procedure, which is the part of CRYSALIS. A detailed list of the reciprocal planes is presented in Sec. VI. The final plane images were averaged over nine adjacent slices, which covered 8% of the lattice constant, e.g., the $hk1.8$ plane was prepared as an average of $hk1.76$ to $hk1.84$ reciprocal planes. Planes with noninteger indices were chosen in order to avoid Bragg peak subtraction.

The RMC calculations for minimizing the difference between the observed and the calculated intensity of the XDS were performed with the DISCUS program.[21] The size of calculation system was chosen to be $26\times26\times31$ unit cells. Our own external procedure was incorporated into DISCUS in order to account for the specific model of disorder. The model and the procedure are described in details in Sec. V. During the RMC refinement the decision on accepting steps was made on the basis of the goodness of fit parameter:

$$\chi^2=\sum_{i=1}^{N}\frac{w(\mathbf{h}_i)\{I_e(\mathbf{h}_i)-[f\cdot I_c(\mathbf{h}_i)+b]\}^2}{\sigma^2}, \tag{1}$$

where $w(\mathbf{h}_i)$ is the weighting parameter, I_e and I_c are the experimental and calculated intensities, respectively, f is a scaling factor, and b and σ are the background and modeling parameters, respectively. The sum in Eq. (1) is taken to be over all considered points of reciprocal space, and the f and b parameters were allowed to change during the simulation.

Every step improving the fit was accepted; otherwise, a $(\Delta\chi^2>0)$ step was accepted with a probability of

$$P_{\mathrm{RMC}}=\exp(-\Delta\chi^2/2). \tag{2}$$

The σ parameter corresponds to the temperature in the standard Monte Carlo scheme. By altering σ, one can manipulate the fraction of good and bad steps that are accepted. In our case σ was chosen such that the fraction of good and bad steps was close to one during the first stage of the calculation (warming up). By the end of the calculation when exploring areas near the fitting minimum, only good steps were accepted. Since some of the planes are situated closer to the Bragg reflections and contain areas of high intensity scattering, it was necessary to apply a weighting in order to avoid the situation where all the efforts of refinement went into fitting only for those relatively few and very intense points.

III. AVERAGE STRUCTURE

A conventional crystal structure analysis performed at two temperatures, 293 and 410 K, confirmed the known structures of the I and I′ phases.[6–10] Some essential details of the structure refinements are collected in Table I.

The structural aspects of the complex disorder of TMA molecules are outside the scope of this paper. However, our calculations showed that, as a first approximation for the TMA disorder at room temperature, the five-well model proposed by Braud *et al.*[8] worked well although the electron density (which was almost uniformly smeared around the nitrogen atoms) could be described using other models. In the high-temperature phase I′, the appearance of additional

TABLE I. Some essential details for the average structure determination of TMCC at room temperature and at 410 K. The hydrogen atoms were omitted in the refinement.

Temperature (K)	Phase	Space group	Lattice parameters a and c (Å)	Atomic parameters atom position		x	y	z	Model of TMA disorder	R_{int}, R, and wR (%)
293	I	$P6_3/m$	9.139(1) 6.723(1)	Cd	2(b)	0	0	0	five-well model	1.2, 2.3, and 4.3
				Cl	6(h)	0.2561(1)	0.1005(1)	1/4		
				N	2(d)	1/3	2/3	3/4		
410	I'	$P6_3/mmc$	9.235(1) 6.742(1)	Cd	2(a)	0	0	0	ten-well model	2.1, 2.8, and 5.6
				Cl	6(h)	0.2562(1)	0.1281(1)	1/4		
				N	2(d)	1/3	2/3	3/4		

symmetry elements indicated that the situation was even more complex.

IV. STATIC VS DYNAMIC ORIGIN OF XDS

In order to explain the origin of XDS, one has to choose between a *dynamic* and a *static* model for the disorder.

Crystal vibrations occur on a time scale ranging from about 10^{-6} to 10^{-14} s, which are small compared to the time scale of an x-ray diffraction experiment. This implies that the observed x-ray diffraction pattern is the time average over all crystal motions. These thermal perturbations are an example of dynamic disorder. By contrast, statically disordered unit cells exist with different arrangements of the time-averaged atomic positions and the interconversion of these arrangements is inhibited by energy barriers that are large compared to kT.[22]

Most structural papers concerned with XDS used only a static model of the crystal, but there are certain known cases where the dynamical approach is needed. A solution for XDS in such crystals was given by Komatsu and Teramoto[18] based on the theory of thermal diffuse scattering (TDS). They showed that in some crystals containing linear or zigzag atomic chains, transverse-acoustic waves were predominantly of low frequency and had wave vectors that were perpendicular to atomic chains. Dynamical displacements of atoms gave rise to a strong TDS, which extended into the sheets perpendicular to the chains direction. Such an approach explained the main features in the diffuse streak patterns observed for a variety of crystals, such as for germanium, white tin, hexagonal ice, adipic acid, and urea. TMCC and other related compounds belong to a group of crystals that could also be studied by such an approach.

The main criterion that enables the recognition of a crystal disordering mechanism is a temperature dependence of the XDS intensity. As shown in Figs. 3 and 4, our measurement results demonstrate that one can distinguish at least three regions where the temperature dependence of the XDS has a different character. On average, the diffuse intensity increased slightly with temperature in the temperature range 180–360 K. However the change had the opposite behavior in the temperature ranges 120–180 K and 360–400 K, which does not support the TDS explanation. Moreover, the XDS intensity reached background levels below 118 K in the ordered monoclinic phase III (Fig. 3, 100 K), which indicated that the $CdCl_6$ octahedra chains became ordered after the I to III phase transition took place. The narrowing of the XDS with decreasing temperature (visible in Fig. 3) can be attributed to both dynamical effects and static crystal ordering.

There are also the following "nondiffraction" arguments for the static disorder of the chains. (i) The analysis of the Raman spectra in phase I of TMMC (Figs. 3 and 6 of Braud

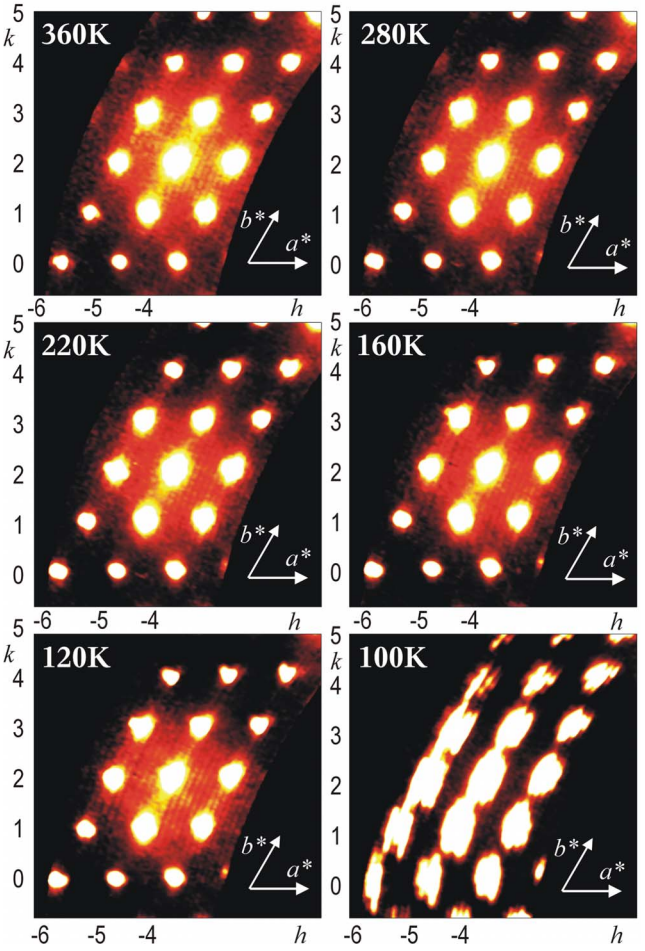

FIG. 3. (Color online) The temperature dependence of the XDS around the $\bar{5}24$ reflection on the $hk4$ layer. At 100 K, the crystal is in the monoclinic phase III (using the same axis description as for the hexagonal cell).

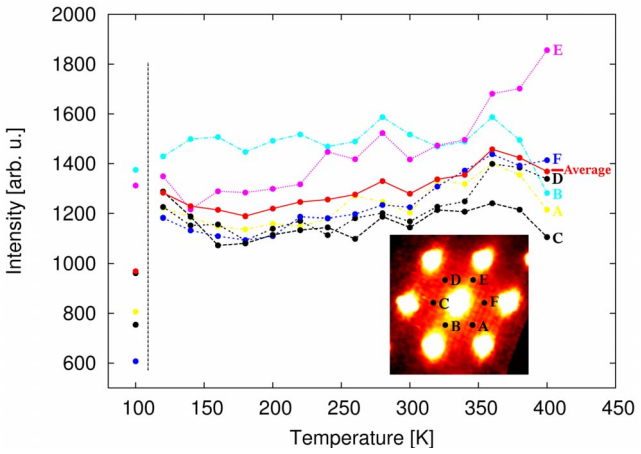

FIG. 4. (Color online) Plot of the XDS intensity value vs temperature for six chosen places around the $\bar{5}24$ reflection on the $hk4$ layer. The phase transition temperature at 118 K is marked by a dashed line. Note that the scattering intensity in points B and E at 118 K is raised by the overlap of twinning Bragg reflections.

et al.[14]) led to the conclusion that the optical bands corresponding to intrachain modes have almost constant half widths vs temperature. (ii) There was a very weak temperature dependence of the translational mode frequency as was shown in Fig. 7 of Braud *et al.*[14] The frequency changed value but the effect was far from the typical mode softening observed due to dynamical effects.

In summary for this section, a detailed analysis of our experimental results indicates that there is a static disorder of the octahedral chains; however, a certain contribution of TDS to XDS, mainly under Bragg reflections, could not be excluded.

V. MODELING AND REFINEMENT

A preliminary modeling of the XDS in TMCC confirmed the conclusion of Braud *et al.*[8] that the main contribution to the XDS came from the static disorder of the $CdCl_6$ octahedral chains. Therefore, any RMC refinement procedure should allow for dividing the infinite chains into subchains of different lengths that can move from their ideal positions in a correlated manner. Expectations that such subchains might be formed spontaneously when allowing all of the Cd and Cl atoms of the modeled crystal to move independently appeared to be unrealistic due to the enormous number of free variables.

Our first attempt of an RMC refinement was of a pure geometrical nature. We postulated a certain distribution of rigid subchains of various lengths and we let them move and change their lengths during the refinement process. The simulation with these geometrical constraints gave a reasonable fit between the experimental and the calculated XDS.

However, our aim was to implement a procedure in which we did not have to force the system to accommodate any given structural pattern but at the same time to bypass the intractable problem of allowing the atoms to move independently during the fitting procedure. Our solution to this problem was a configurational-bias reverse Monte Carlo technique (CBRMC) with a two-step scheme of accepting each change in the atomic configuration. In the first step, a bias for the common RMC procedure was introduced in order to check whether a given trial was relevant from the structural point of view. In the second step, final acceptance was made depending on the RMC goodness of fit parameter.

To allow the system to distort the $CdCl_6$ octahedra and evolve almost freely during the refinement, we divided the chains into small elementary blocks that consisted of one Cd atom and three adjacent Cl atoms [see Fig. 1(b)]. Each block was associated with a vector $\mathbf{s}$, which represented the shift from the average position (we assumed that the shifts were not bigger than 0.1 Å in the a and b direction and were not bigger than 0.12 Å in the c direction). The change in $\mathbf{s}$ defined one MC step.

The full scheme of one CBRMC step is as follows: (i) choose randomly one block and the shift vector ($\mathbf{s}_i^{\text{new}}$); (ii) accept the trial with a probability of P_{bias}, and if the trial is not accepted, go back to (i); (iii) calculate the scattering intensities and accept the step with a probability of P_{RMC}. In our calculations, the starting configuration consisted of random shifts. The simulation was performed until no change in the χ parameter could be achieved, which required a total number of 2×10^6 CBRMC steps.

The model of biasing has been constructed to favor correlated shifts of the neighboring blocks along the c direction. We defined the function to be minimized for the ith block as

$$U_i = -J_z \mathbf{s}_i \cdot (\mathbf{s}_{i+1} + \mathbf{s}_{i-1}), \tag{3}$$

where J_z represents a coupling constant and $i \pm 1$ indicate the nearest neighbors in the column extending along the c direction. The bias probability for the trial $\mathbf{s}_i^{\text{new}}$ is as follows:

$$P_{\text{bias}} = \min\{1, \exp[-(U_i^{\text{new}} - U_i^{\text{old}})/kT]\}. \tag{4}$$

Despite its simplicity, this model was capable of describing the coupling between the orientation of a TMA molecule and the local modification of the octahedral chain. As shown in Fig. 1, a certain configuration of a TMA molecule can locally influence the three neighboring octahedra due to the existence of O-H···Cl hydrogen bonds connecting the TMA molecules and the $CdCl_6$ octahedra. The division of each individual octahedron into two independent halves has opened the possibility to model flexible octahedra, which seems to be more realistic than the rigid chain model applied by Braud *et al.*[8]

VI. RESULTS AND DISCUSSION

A selection of eight of the twenty refined reciprocal planes together with the experimental data is collected in Fig. 5, whereas a full set of planes is presented in Table II. We have found excellent agreement between the observed and the calculated patterns, and all characteristic features of XDS were reproduced in the calculated pattern. In Fig. 5, we have chosen only those planes that reveal very strong diffuse effects, among them, the $h0.75l$ plane, which displays the worst fit between the calculated and the experimental intensities in the whole set. The total R factor is 26.4%, which

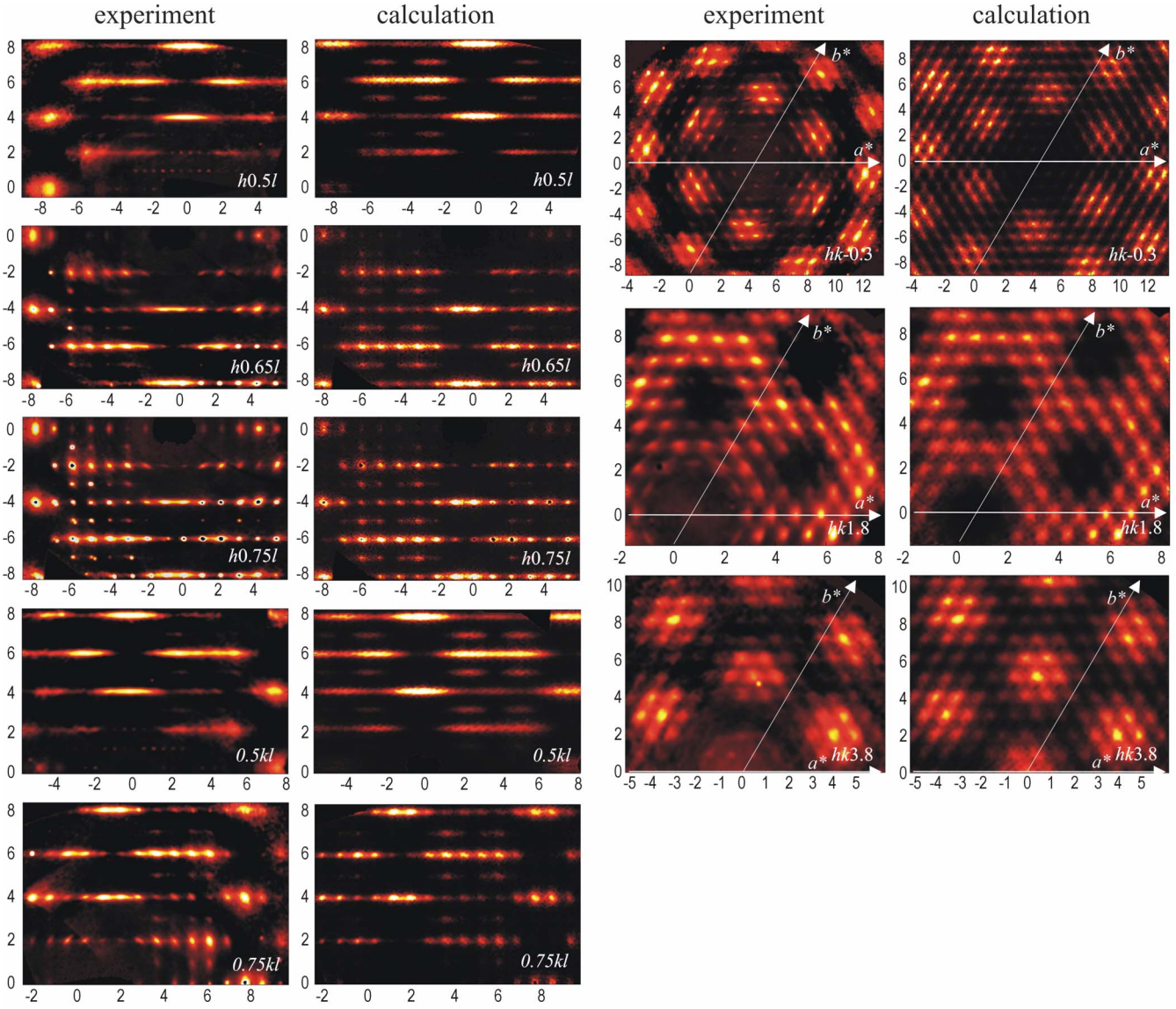

FIG. 5. (Color online) Comparison of the experimental (left) and calculated (right) distributions of the XDS in eight of 20 reciprocal space sections taken for the refinement of TMCC at room temperature. Note that both the $h0.5l$ and $0.5kl$ experimental sections contain weak but sharp peaks forming layers that arise from the second harmonics at the x-ray radiation wavelength.

seems to be large when compared with routine crystallographic refinement. However, one has to realize that in this case, we are fitting over 2.1×10^6 data points, which is hundreds of times the number of Bragg reflections that are fitted in standard x-ray experiments. Furthermore, planes that are close to an integer contain high intensity areas that might be affected by the tails of Bragg spots and thus are difficult to fit.

The corresponding sections of the resulting crystal are shown in Fig. 6. Correlational effects along c direction are clearly visible in the ac section [Fig. 6(a)]. The independent blocks form extended subchains that can be shifted up [sequences of dark (blue) arrows] or down [sequences of grey (pink) arrows] from their average positions.

The subchain length distribution, together with the correlation function for the z component of **s** (i.e., the longitudinal correlation), are presented in Fig. 7. From the Poisson-like distribution, we found the average length of the subchains to be about six unit cells, which was distinctly smaller than the length of 18 unit cells predicted by Braud *et al.*[8] Similarly, the intersubchains transverse correlation (in the directions perpendicular to c) was lower, yielding a few unit cells [see Fig. 6(b), where the unicolor areas are extended not much more than for 4–5 blocks]. However, both effects contribute to the XDS in the way presented in Ref. 8: the strong intrachain longitudinal correlation causes the appearance of a finite width in the diffuse scattering planes perpendicular to c^*, whereas the transverse correlation results in a weak modulation of the XDS intensity [see Figs. 2(e) and 2(f)].

As already pointed out, there are also two additional diffraction effects that were previously not recognized, namely: (i) the XDS on $hk0$ plane [Fig. 2(a)] and (ii) the diffuse streaks visible on and in the vicinity of the hkl planes, with $l=2n$ [Fig. 2(f)]. To explain the first phenomenon, we al-

TABLE II. A list of the reciprocal space sections taken for the refinement of the local crystal structure of TMCC at room temperature, together with a number of experimental points for each section and the weighting scheme applied. The R factors describe the fitting between the calculated and the experimental XDS intensities and are calculated according to the formula: $R=\sqrt{\chi^2/\Sigma w I_e^2}$.

Reciprocal space plane	Number of points	R factor [%]	Weighting scheme
$hk0.25$	382×392	26.3	1
$hk0.3$	288×232	27.6	1
$hk0.35$	405×427	31.2	1
hk-0.3	467×432	30.5	1
$hk1.3$	263×265	24.3	1
$hk1.75$	333×270	30.4	1
$hk1.8$	265×245	24.9	1
$hk2.8$	302×283	35.7	1
$hk3.8$	304×232	24.2	1
$h0.5l$	408×287	18.9	1
$h0.6l$	470×280	17.3	1/Int
$h0.65l$	384×275	31.5	1/Int
$h0.7l$	402×278	21.7	1/Int
$h0.75l$	385×278	36.1	1/Int
$0.5kl$	424×281	17.2	1
$0.75kl$	362×274	28.0	1/Int
$0.8kl$	419×255	21.3	1/Int
$3.5kl$	337×257	32.1	1
$3.6kl$	333×256	31.8	1/Int
$3.7kl$	329×256	35.7	1/Int

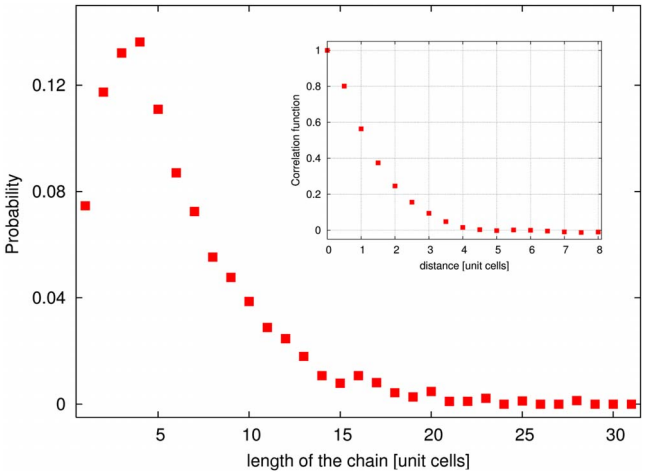

FIG. 7. (Color online) The subchain length distribution (i.e., the probability of finding the block in a chain of a given length) and the correlation function for the z component of blocks displacement vector **s** (inset) for TMCC at room temperature.

lowed the blocks (and consequently the subchains that were formed) to shift within the ab plane. The resulting structures indicate that the appearance of uncorrelated transverse displacements of the subchains is a sufficient condition to produce the proper scattering distribution on the $hk0$ plane. The explanation for the presence of both strong and weak modulations on the $hk0$ plane is the same for the other reciprocal planes perpendicular to c^*. A second effect, the existence of streaks, is related to the transverse correlation gain for certain crystallographic directions in the ab planes, i.e., [100], [010], and [110], which generate planar objects that are parallel to the c axis and can consist of up to 10 subchains that

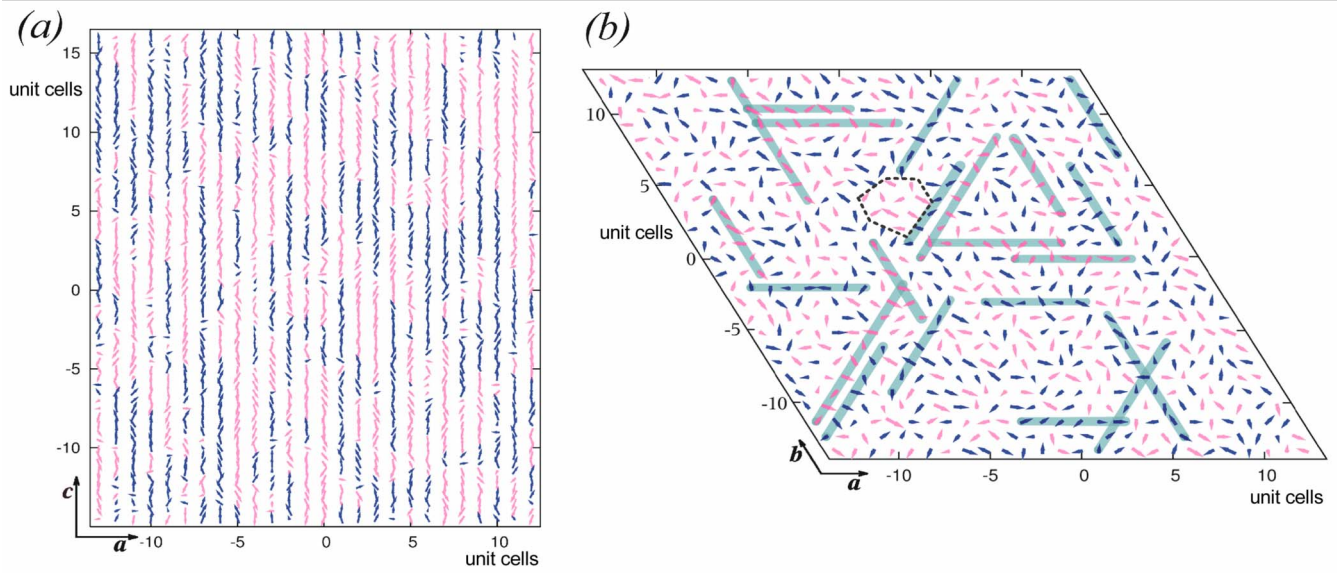

FIG. 6. (Color online) Results of the RMC refinement on the chain disorder in TMCC at room temperature. Two sections of the resulting crystal are presented: (a) ac-plane for $y=0$ and (b) ab-plane for $z=0$. Arrows denote the direction and magnitude (distinctly exaggerated in relation to the unit cell dimensions) of the displacement **s** for each block. Colors denote the sense of the z component of the displacement: dark (blue)=shift up ($s_z>0$); grey (pink)=shift down ($s_z<0$). In (b) two characteristic types of objects causing the XDS effects are shown: (i) a large domain of unidirectional shifts (indicated by a dotted line) and (ii) a set of stripes extending along the [100], [010], and [110] directions. Note that (a) is elongated in the c direction to make the picture more readable.

are equally shifted in *c* direction. Linear sections of these objects with the *ab* plane are indicated in Fig. 6(b) by grey (light blue) stripes.

As revealed by Rodriguez *et al.*,[9] a structural phase transition in TMMC at 126 K occurs due to the ordering of the TMA molecules. The unit cell is doubled in *b* by alternating shifts of the $CdCl_6$ chains along *c* direction. Therefore, the structure contains alternating infinite planes of equally shifted chains of octahedra. From this point of view, the transverse correlation observed by us at room temperature, which led to the appearance of the previously mentioned planar objects, can be interpreted as a precursor effect of low-temperature structure ordering.

The CBRMC procedure was also applied to the data collected in the phase I′ (410 K). As we have already seen, there is a symmetry gain in the high-temperature phase—which is also true for the XDS. Additional mirror planes result from the rotation of the $CdCl_6$ octahedra, and there are no other structural effects involved. Thus, the exact same procedure was used here, which yielded qualitatively the same results as those found for phase I. The corresponding reciprocal planes are shown in Fig. 8.

Since our experimental data does not support the TDS-based explanation for the diffraction effects observed in TMCC, we treated the structures resulting from refinement as statically disordered. However, this is not in contradiction with the dynamical approach if the structures are regarded as "snapshots" of the dynamically perturbed structure rather than statically displaced chains.

VII. CONCLUSIONS

We have re-examined the static model of $CdCl_6$ octahedral chain disorder in TMCC using the reverse Monte Carlo method with a configurational-bias flavored scheme of sampling. As a result of our extended data refinement (taking into account a set of 20 reciprocal space sections containing over 2.1×10^6 experimental points), we obtained excellent agreement between the diffraction experiments and the calculations. The resulting structures contain highly correlated subchains that are shifted from the average positions and have a Poisson-like distribution for their length with an average value of about six unit cells. X-ray diffuse scattering observed on the *hk*0 plane requires the existence of subchain displacements in the *a* and *b* directions, which was neglected in previous studies. An additional transverse correlation between the subchain shifts was needed in order to account for the diffuse streaks observed on the planes perpendicular to c^*. We have found that the symmetry of the x-ray diffuse scattering was consistent with the symmetry of the average structure for phases I and I′, and the same kind of structural disorder could be recognized for both phases.

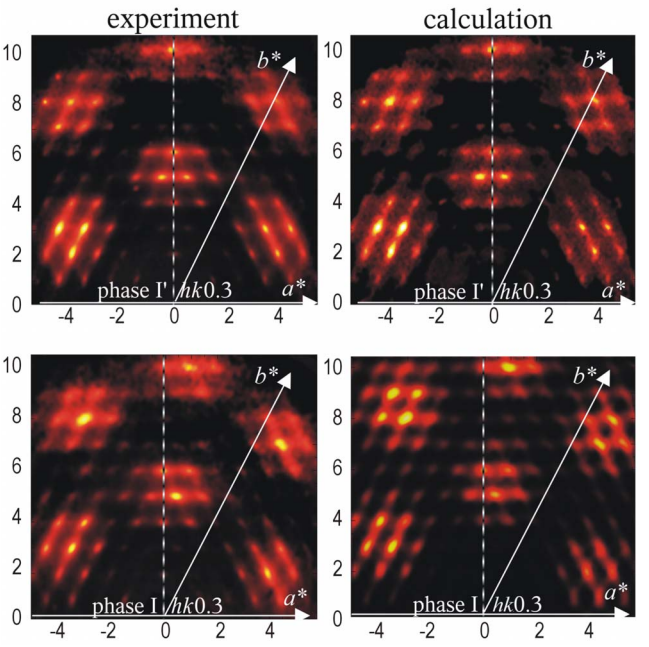

FIG. 8. (Color online) Comparison of the experimental (left) and calculated (right) distributions of the XDS for the *hk*0 plane of phase I (293 K) and phase I′ (410 K) for TMCC. The dotted lines indicate the mirror plane of phase I′.

The configurational-bias reverse Monte Carlo method proved to be a very efficient tool for modeling the effects of disorder on x-ray diffuse scattering experiments. Furthermore, this approach is, in our opinion, a step toward the method of refinement of three-dimensional diffraction data, which would be free of any intuitively devised structural constraint.

By analyzing the temperature dependence of the XDS intensity and the half widths of selected Raman bands, we excluded dynamic disorder as being the main factor responsible for the observed XDS effects. However, there is some experimental evidence that could indicate a weak contribution from dynamic effects.

ACKNOWLEDGMENTS

This work was supported by the Polish Ministry of Education and Science from the budget funds for science 2005-2008 as a Grant No. 3 T09A 164 28. M.P. would like to thank the IMPRS "Dynamical Processes in Atoms, Molecules and Solids" in Dresden and the Klaus Tschira Foundation (Heidelberg) for his scholarship. We would like to thank Stefano Leoni for the valuable discussions.

[1] P. S. Peercy, B. Morosin, and G. A. Samara, Phys. Rev. B **8**, 3378 (1973).
[2] R. E. Caputo and R. D. Willett, Phys. Rev. B **13**, 3956 (1976).
[3] T. T. P. Cheung, Z. G. Soos, R. E. Dietz, and F. R. Merritt, Phys. Rev. B **17**, 1266 (1978).
[4] F. Borsa, M. G. Pini, A. Rettori, and V. Tognetti, Phys. Rev. B **28**, 5173 (1983).
[5] N. F. Wright, M. D. Johnson, and M. Fowler, Phys. Rev. B **32**, 3169 (1985).
[6] B. Morosin, Acta Crystallogr., Sect. B: Struct. Crystallogr. Cryst. Chem. **28**, 2303 (1972).
[7] N. W. Alcock and S. L. Holt, Acta Crystallogr., Sect. B: Struct. Crystallogr. Cryst. Chem. **34**, 1970 (1978).
[8] M. N. Braud, M. Couzi, N. B. Chanh, C. Courseille, B. Gallois, C. Hauw, and A. Meresse, J. Phys.: Condens. Matter **2**, 8209 (1990).
[9] V. Rodriguez, G. Aguirre-Zamalloa, M. Couzi, and T. Roisnel, J. Phys.: Condens. Matter **8**, 969 (1996).
[10] I. Peral, G. Madariaga, A. Perez-Etxebarria, and T. Breczewski, Acta Crystallogr., Sect. B: Struct. Crystallogr. Cryst. Chem. **56**, 215 (2000).
[11] Y. Tazuke, J. Phys. Soc. Jpn. **42**, 1617 (1977).
[12] Y. Mlik and M. Couzi, J. Phys. C **15**, 6891 (1982).
[13] M. T. Hutchings, G. S. Pawley, and W. G. Stirling, J. Phys. C **16**, 115 (1983).
[14] M. N. Braud, M. Couzi, N. B. Chanh, and A. Gomez-Cuevas, J. Phys.: Condens. Matter **2**, 8229 (1990).
[15] M. N. Braud, M. Couzi, and N. B. Chanh, J. Phys.: Condens. Matter **2**, 8243 (1990).
[16] J. Diaz-Hernández, G. Aguirre-Zamalloa, A. López-Echarri, I. Ruiz-Larrea, T. Breczewski, and M. J. Tello, J. Phys.: Condens. Matter **9**, 3399 (1997).
[17] G. Aguirre-Zamalloa, V. Rodriguez, M. Couzi, F. Sayetat, and P. Fertey, J. Phys.: Condens. Matter **9**, 937 (1997).
[18] K. Komatsu and K. Teramoto, J. Phys. Soc. Jpn. **21**, 1152 (1966).
[19] M. Sheldrick, SHELX-97, program for crystal structure solution and refinement, University of Göttingen, 1997.
[20] CRYSALIS software, Version 170.30.6, Oxford Diffraction Ltd., 2007.
[21] T. Proffen and R. B. Neder, J. Appl. Crystallogr. **30**, 171 (1997).
[22] D. S. Moss, G. W. Harris, A. Wostrack, and C. Sansom, Crystallogr. Rev. **9**, 229 (2003).